

Article

Time Delay Characterization in Wireless Sensor Networks for Distributed Measurement Applications

Šarūnas Kilius ^{1,*}, Darius Gailius ², Mindaugas Knyva ¹, Gintautas Balčiūnas ², Asta Meškuotienė ² ,
Justina Dobilienė ² , Simas Joneliūnas ³ and Pranas Kuzas ¹ 

¹ Department of Electronics Engineering, Kaunas University of Technology, Studentu Str. 50-457, 51368 Kaunas, Lithuania; mindaugas.knyva@ktu.lt (M.K.); pranas.kuzas@ktu.lt (P.K.)

² Metrology Institute, Kaunas University of Technology, Studentu Str. 50-454, 51368 Kaunas, Lithuania; darius.gailius@ktu.lt (D.G.); gintautas.balciunas@ktu.lt (G.B.); asta.meskuotiene@ktu.lt (A.M.); justina.dobilienė@ktu.lt (J.D.)

³ Independent Researcher, Kalpoko Str. 29, 44146 Kaunas, Lithuania; simas.joneliunas@gmail.com

* Correspondence: sarunas.kilius@ktu.lt

Abstract: This paper investigates the critical aspect of synchronization in wireless sensor networks (WSNs) across diverse industrial applications. The low-cost sensor network topologies are analyzed. The communication delay measurements and quantitative jitter analysis are performed under different conditions, and dependencies of the propagation time delay on the data bitrate and modulation type for different hardware implementations of the WSNs are presented. The time delay distribution influence on the time synchronization error propagation over WSN layers was assessed from the experimental probability density functions. The network synchronization based on the controlled propagation delay jitter approach has been proposed. This research contributes quantitative insights into the complexities of synchronization in WSNs, offering a foundation for optimizing network configurations and parameters to extend the operational life of low-power sensor nodes.

Keywords: low-cost sensor network; wireless sensor networks; quantitative jitter analysis; communication delay



Citation: Kilius, Š.; Gailius, D.; Knyva, M.; Balčiūnas, G.; Meškuotienė, A.; Dobilienė, J.; Joneliūnas, S.; Kuzas, P. Time Delay Characterization in Wireless Sensor Networks for Distributed Measurement Applications. *J. Sens. Actuator Netw.* **2024**, *13*, 31. <https://doi.org/10.3390/jsan13030031>

Academic Editor: Lei Shu

Received: 9 April 2024

Revised: 8 May 2024

Accepted: 13 May 2024

Published: 16 May 2024



Copyright: © 2024 by the authors. Licensee MDPI, Basel, Switzerland. This article is an open access article distributed under the terms and conditions of the Creative Commons Attribution (CC BY) license (<https://creativecommons.org/licenses/by/4.0/>).

1. Introduction

Wireless sensor networks (WSNs) are widely used in modern distributed data acquisition solutions. Integration of the intelligent metrology systems in Metrology 4.0 solutions enables a rich spectrum of WSN applications along with integration to the Internet of Things (IoT) network: smart water meters [1] and smart electricity metering systems [2] equipped with ZigBee modules and connected to WSNs. In the human safety area, WSNs are used for the implementation of metal mine underground safety systems [3] and wildlife detection and signaling on road systems [4]. In the brewage industry, ZigBee WSN was used to monitor the changes in the winery's environment [5]. In the weaving industry, the WSN is used for monitoring and direct load controlling for efficient power utilization [6]. The role of WSNs in an industrial environment is especially growing in regards to the growth of digital Industry 4.0. Safa Saadaoui et al., in their work [7], described the benefits of industrial wireless sensor networks (IWSN) and presented simulations of architectures. Besides being widespread in the industry and research areas of WSNs, the active lifetime of battery-powered nodes of IoT networks is defined by the node active time. At the protocol level, the data packet contains overhead, which is necessary for the implementation of the transmission and error control. The communication time window width when the receiver or transmitter must be kept powered and active for each node is defined by the used protocol, number of nodes in the network, network structure, etc. These aspects affect the WSN life cycle and can be controlled using proper configuration and optimization either at the protocol or hardware level. The WSN synchronization among the nodes is

required to keep the measurement timing for the applications that demand a solid time base for distributed measurements:

- Coherent sensors. For example, remote high-speed measuring devices where synchronous measuring at multiple distributed autonomous points is required;
- Acoustic emission measurement system where precise time marks are required for further data processing of measured data [8] (see Figure 1);
- Wireless ECG sensors measurement system where synchronization between measurement points is needed [9] (see Figure 2);
- Low-power distributed wireless sensor grids, in many cases, require precisely synchronized timers to minimize the power consumption required to keep active RX channels [10–13].

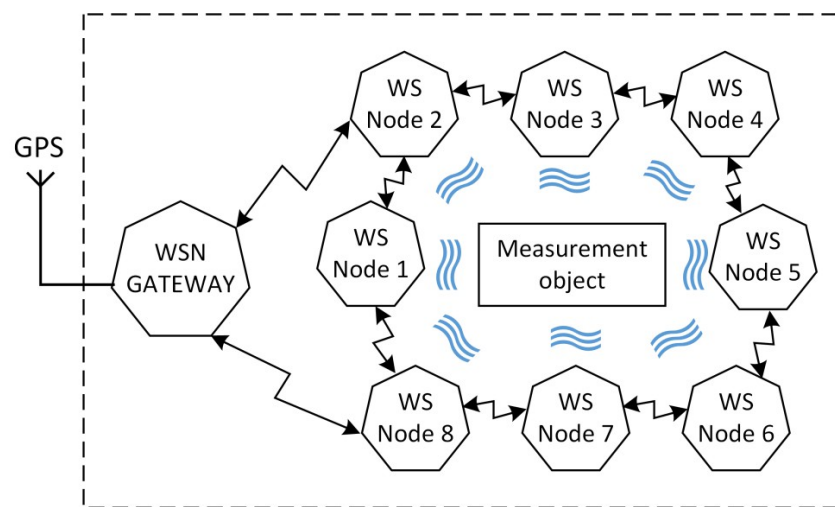


Figure 1. WSN structure with receiver–receiver synchronization.

Various synchronization protocols such as NTP, PTP, RBS, and TDP [14–17] have been proposed by researchers to help synchronize wireless measurement nodes in the network. Protocols work differently and have different synchronization accuracy and energy consumption, introducing different synchronization errors. Nguyen, V.-H. et al. [18] present a hybrid routing protocol called HRP-EE for wireless sensor networks (WSNs) in the context of Internet of Things (IoT) applications. The protocol aims to optimize energy consumption and prolong the network’s operational lifespan. It utilizes cluster-based approaches, Voronoi diagrams, and algorithms such as Minimum Spanning Tree (MST) and Dijkstra to enhance energy efficiency and network longevity. Compared with other protocols, HRP-EE demonstrates its superiority in terms of energy efficiency, network lifespan, and data packet delivery. Verma, S. et al. [19] propose a framework called Sleep scheduling-based Energy Optimized Framework (SEOF) to address the limited energy resources of sensor nodes deployed in IoT-based WSNs for wildfire detection. The framework includes an energy-efficient Cluster Head (CH) selection using a Tunicate Swarm Algorithm (TSA) and a sleep scheduling methodology for closely located sensor nodes. The simulation results show that SEOF improves the network stability period for different scenarios by 35.3% and 216% compared to CIRP. Faheem, M. et al. [20] introduce a lightweight smart contracts framework for secure communication in smart grid applications, focusing on blockchain technology implementation in smart grid data communication and sharing. The framework aims to enhance security and integrity in information transmission between entities in the smart grid. Through private Solana blockchain architecture, secure smart contracts, and simulation studies, the proposed Advanced Solana Blockchain (ASB) scheme demonstrates effectiveness in securing data sharing.

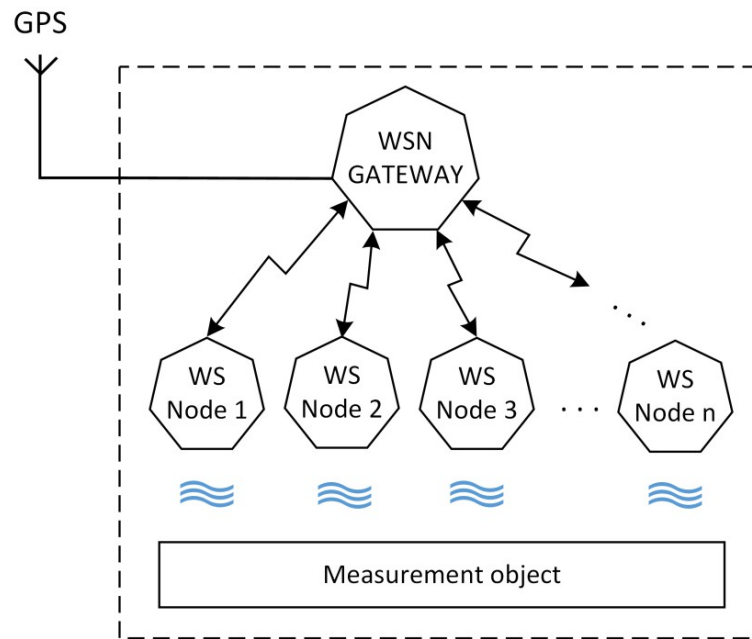


Figure 2. WSN structure with sender–receiver synchronization.

Electric energy accounting solutions require synchronization and assessment of the derived parameters, such as the remote meter error determination or cases of electrical energy theft that are possible using synchronized networks [21,22]. The synchronization accuracy also depends on the implementation of the WSN node software [23]. One of these errors is sender-induced delay, which was described by Kulakli et al. [24]. It can be reduced or even eliminated using receiver–receiver [25] type synchronization protocols, but in sender–receiver [26] protocols, it cannot be avoided. In Figures 1 and 2, WSN structures of sender–receiver and receiver–receiver are shown.

Figure 1 represents the example of a WSN with synchronization performed using a receiver–receiver structure. Here, the gateway forms a synchronization message using a GPS signal (or other available time service can be used) and sends it to the nearest wireless sensor nodes. Synchronization messages are resent using wireless nodes as routers from node to node.

Figure 2 represents WSNs configured using a sender–receiver structure. Here, the gateway forms synchronization messages using a GPS signal. Each network node communicates with the gateway directly. So, in this case, synchronization is provided directly. The wireless sensor transceiver implementation at the hardware level, however, introduces the delay variation with each packet transmission. During the initialization stage of the network, the synchronization protocol-built time base is usually based on the limited amount of transmissions (e.g., four transmission cycles and eight timestamps for the PTP protocol) to set the time base for the section or whole WSN.

M. Knyva et al., in their paper [4], described a method for wild animal detection near the roads. For animal detection, IoT sensor nodes mounted on the road poles were used. Each node is equipped with a solar panel and pack of batteries as the main power supply. The LPWAN network was formed using LoRa modulation. The concrete network application scenario for the wild animal detection in the trunk road section installed on the Kaunas–Šakiai (41 km) road section is presented in Figure 3. It is comprised of digital sensor nodes (DSN1–DSN8). The DSN1 node serves as the gateway in this particular application. The sensor nodes stay in deep sleep mode until the animal is detected. After the detection event is triggered, the node sends a signal to the gateway. This network configuration works perfectly if the distance between the gateway and a sensor node is up to 1 km. (The road goes through the forest in the investigated case.) For extension of the network range, the re-transmitters waking at a priori known time moments can be used.



Figure 3. Animal detection IoT network with the implemented placement of the DSN nodes.

The lack of a priori knowledge of the quantitative delay parameters and statistical characteristics of the time delay variation, according to the authors' experience, may significantly deteriorate the performance of the WSN due to several aspects. The variation in the time delay limits the low power mode duration of the WSN nodes, as they must be programmed to keep the RX active for a longer time to receive the data. In the multi-layered network configuration, where the time base cannot be set directly from the WSN gateway, the time delay variation increases at each layer in the case of fixed time base setting communication cycles. The usage of different hardware transceiver nodes (focused on low-cost solutions) induces the uncertainty of the induced time delay and, therefore, motivates the dedicated research to find out the HW-induced time delay and jitter estimates. In this paper, authors present time synchronization error quantitative and statistical characterization induced by hardware measured during experiments with WSN using various ISM band low-cost transceivers. The hardware-focused time delay assessment for reducing the time delay variation spread is discussed.

The main objectives of this study are as follows:

- Investigate the various delays involved in time synchronization in wireless sensor networks (WSNs) for precise measurements, including send delay, channel access delay, transmission delay, propagation delay, receive delay, and processing delay;
- Measure the communication delay and analyze the quantitative jitter using different conditions and dependencies such as data bitrate, modulation type, and hardware implementations of WSNs;
- Assess the influence of time delay distribution on the time synchronization error propagation over WSN layers and provide quantitative insights into the complexities of synchronization in WSN.

2. Synchronization Time Delay

Synchronization between two WSN nodes can be described as a comparison process of the clocks. Typically, the reference clocks (in most cases based on crystal oscillators) slightly differ in frequency. The difference in temperature of operation and varying voltage of the WSN node internal battery result in different drifts of the clocks, and therefore, periodical resynchronization of the WSN is needed. While a synchronization packet is formed and sent from one node (for example, gateway) to another node (for example, wireless sensor node), some delays may appear. These delays must be characterized, and their sources identified and analyzed. Some characteristics of the packet delays between sender–receiver nodes were given by Liu et al. [26]. Their approach to the time delay description is composed of the separate stages of information packet propagation through the WSN node. The send delay refers to the construction of a synchronization message and submits the sending packet to the MAC layer. Channel access delay is random and depends on the current channels' status—idle or busy. The transmission delay defines the time it takes for the sending node to transmit the message to the antenna. On the receiver

side, the receive delay (the hardware-induced delay constituent) and processing delay (the induced delay constituent) are identified.

During the design stages of the WSN, various approaches can be made to assign the message-receiving moment. Since the software (firmware) solutions in the WSN microcontroller may vary in the method and moment of received packet processing, in this paper, the research is aimed at the transceiver hardware induced delay. The motivation for research arises from the authors' experience with different transceiver solutions of various manufacturers. The authors identified hardware and modulation type-dependent delay jitter of the transceiver when it is working in transmission or reception mode. Power usage and measurement result acquisition synchronization precision can be considerably improved using the delay time range prediction in the early design stages of the low-power WSNs.

The chosen hardware setup replicates the communication channel of the WSN section. It consists of a transmitter and receiver pair. The microcontroller software is programmed to send repetitive synchro packet data (or network payload data) messages with chosen settings (modulation, message structure, and other transceiver-related settings) over the investigated transceiver pair. The transceiver hardware-driven flag (output pin level change) was chosen for the time delay measurement experimental research. Figure 4 shows the proposed characterization of the time delay and jitter in WSN.

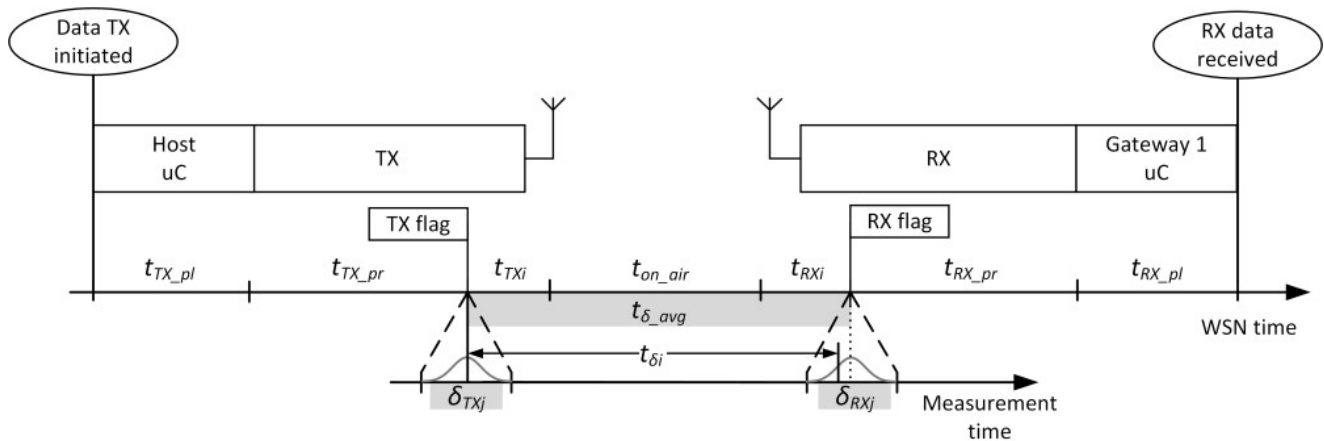


Figure 4. WSN time delay characterization for WSN communication channel.

The event sequence of the data packet transmission process between two adjacent WSN network nodes is shown in Figure 4. The software processing-induced time delay in the TX firmware is until the TX flag event; as for the receiver RX, the software processing is performed after the RX flag event. The network events are displayed on the WSN time base; the measured HW delay $t_{\delta i}$ is acquired using the measurement instrument (LeCroy HRO 66Zi). The measurement time base is relative to the TX flag moment.

At the sending WSN node, after the packet is acquired, the data packet prepared by the microcontroller is sent to the transceiver hardware via the SPI interface (TX data payload time interval t_{TX_pl} in Figure 4). After the packet header, preamble, and other necessary information are added in the transceiver (TX process delay interval t_{TX_pr} in Figure 4), the TX flag of the sending transceiver IC hardware pin is set to indicate the “PACKET TRANSMITTED” state.

During TX operation, the TX flag is set after the packet is sent to the RF amplifier stage to be transmitted to the antenna. This time interval is denoted as t_{TXi} in Figure 4. The randomly distributed TX jitter δ_{TXj} , depending on the hardware solution of the transceiver, is introduced. The packet on-air time t_{on_air} is radio wave propagation delay, which depends on the transmission path distance. During the time base synchronization and resynchronization procedures, the time on air delay constituent t_{on_air} can be considered as a constant for the pre-mounted transceiver–receiver pair setup. On the receiving WSN

node side, the received data packet is analyzed and processed in transceiver hardware—the preamble, header, etc., are removed. This procedure contributes to the delay t_{TXi} . After the hardware level processing is finished, the RX hardware flag is set. In this work, the “RX DONE” flag was chosen as the RX flag for the cumulative propagation delay and RX jitter assessment (see Figure 4). The RX process delay $t_{RX_{pr}}$ is introduced by the RX hardware before sending the packet data to the receiver microcontroller through the SPI bus. The data payload processing is performed in the RX (or gateway) microcontroller, which is denoted as delay $t_{RX_{pl}}$.

3. Time Delay Distribution Assessment

The measured delay time interval at the i -th measurement $t_{\delta i}$ between WSN nodes’ TX flag raised and the RX flag raised for the WS network with two nodes can be defined:

$$t_{\delta i} = t_{TXi} + t_{on_air} + t_{RXi}, \tag{1}$$

where t_{TX} is the TX delay of transmitter hardware, t_{on_air} is time on air delay, and t_{RX} is RX delay of the receiver hardware (see Figure 4).

Full-time delay t_{nodei} (packet formed at sending node SW and packet decoded at receiving node SW) for i -th transmission of the synchronization message can be expressed:

$$t_{nodei} = t_{\delta i} + t_{TX_{pl}} + t_{TX_{pr}} + t_{RX_{pl}} + t_{RX_{pr}}, \tag{2}$$

where $t_{\delta i}$ is the experimentally measured time delay during i -th measurement. $t_{TX_{pl}}$ is TX payload preparation delay, $t_{TX_{pr}}$ is duration of payload data processing through transmitter, $t_{RX_{pl}}$ is RX received data and payload forming delay, and $t_{RX_{pr}}$ is data decoding and processing delay.

For the WS network with j layers, the absolute delay t_{nodeij} at i -th transmission of the synchronization message $data_{sync_j}$ arrival regarding the WSN gateway time base (Figure 5) can be expressed as follows:

$$t_{nodeij} = \sum_j (t_{\delta ij} + t_{TX_{pl}} + t_{TX_{pr}} + t_{RX_{pl}} + t_{RX_{pr}}). \tag{3}$$

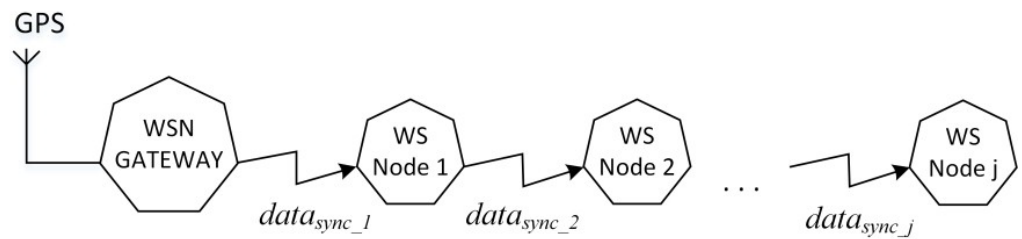


Figure 5. WSN synchronization message propagation in the WSN.

All delays except $t_{\delta i}$ depend on the WSN node microcontroller software implementation. The variance in the time delay $t_{\delta i}$ at the j -th WSN layer consists of two parts: δ_{TXj} and δ_{RXj} . The differential measurement setup is provided with the TX flag as the reference; therefore, in the experiment data, the variations in the time delay induced by the TX hardware δ_{TXj} and induced by the RX hardware δ_{RXj} are inseparable; hence, for the j -th layer of the WSN, the combined jitter is as follows:

$$\delta_{TRXj} = \sum_j (\delta_{TXj} + \delta_{RXj}). \tag{4}$$

Uncertainty of the time delay when sending the predefined data packet between TX and RX can be estimated, and the delay time is assessed from the experimental data. Estimation of the transmission delay t_{nodei} and combined jitter δ_{TRXj} for distributed low data rate WSN nodes can be used as a reference for optimizing the network configuration and parameters. The experimental datasets are acquired and analyzed in this work in

terms of statistical distributions for assessment of the conjoined hardware-dependent RX jitter δ_{TRXj} . The influence on the RX jitter induced by modulation types and data rates is analyzed for the same type of transceivers, as well as differences for transceivers from different manufacturers.

For evaluation of the propagation of the RX jitter δ_{TRXj} , over the WSN, the structure of the WSN presented in Figure 5 is synthesized. It consists of the consequent chain of communication channels between the WSN nodes through which the synchronization message $data_{sync_j}$ is retransmitted.

The received i -th synchronization message introduces an absolute delay t_{nodeij} (Formula (3)), which increases with each consequent WSN layer. The jitter δ_{TRXj} also increases. For investigation of the control of the jitter δ_{TRXj} , the modeling based on the measured data in the MATLAB software was set. The model assumes that the jitter has experimentally measured unique distribution and that the jitter δ_{TRXj} distribution from the previous WSN layer is convoluted with the jitter distribution of the subsequent layer. The method of partial control of the jitter proposed by the authors is included in the model. The proposed method consists of processing the experimentally measured hardware time delay jitter raw data $t_{\delta i}$. The accumulated measured result array size $N = 200,000$ independent measurements were acquired by using the measurement system setup presented in Figure 6. The measured data are used for the first layer time delay jitter definition. The following layer jitter data are derived from the previous layer jitter data. The assumption is made that using a very large amount of experimental measurement samples (200,000 or more samples) for the simulation of the further layers would not significantly affect the quantitative parameters of statistical parameters used for the definition of the time delay jitter propagation.

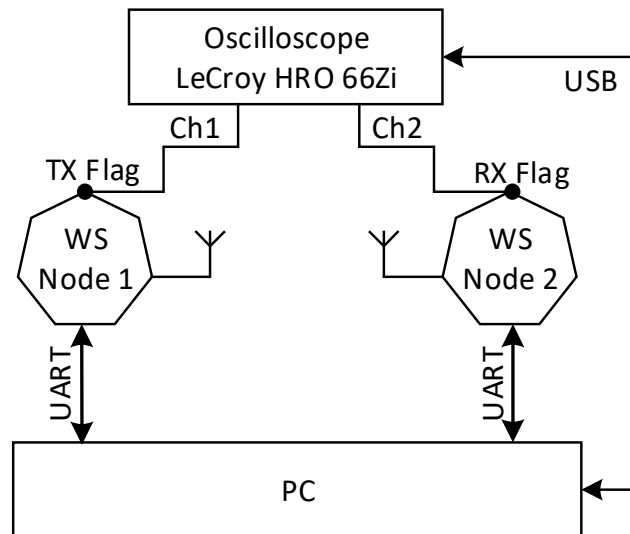


Figure 6. Experimental setup for time delay distribution characterization.

For the simulation of the time delay jitter propagation over the WSN layers in the MATLAB software, the concept of control of deviation of the time base parameters was implemented. The intermediate dataset for estimating the jitter δ_{TRXj} at the j -th layer of the WS network JJ is simulated from the dataset of raw measurement dataset $t_{\delta}[N]$ by generating a data array for each layer:

$$JJ[j, N] = t_{\delta}[rand(N)], \tag{5}$$

where t_{δ} is the time delay experimental measurement database; j is the number of the simulated WS network layer; $rand$ is the uniform distribution random index number generating function from the population of N samples ($N = 200,000$).

The dataset RS for estimation of the statistical parameters of the time delay jitter in the j -th layer of the simulated network is generated:

$$RS_j[N] = \frac{1}{j} \sum_{k=1}^j JJ[k, N]. \quad (6)$$

The approach using the method from Formulas (5) and (6), assumes the linearly increasing amount of the synchronization messages $data_{sync_j}$ over the j -th WSN layer. From the network resources point of view, the synchronization (and resynchronization) procedure duration increases linearly depending on the current network layer. From the time base uncertainty point of view, the proposed approach enables controlling the jitter raise through the network layers. In special cases, depending on the need for synchronization of the given layer of the WSN, the number of synchronization messages can be increased nonlinearly.

The measured and mathematically modeled time delay histograms are hardware-dependent. Under this circumstance, the case study was performed by implementing the WSN transceivers investigated by the authors and applying the simulation of the jitter data (Equations (5) and (6)).

The statistical parameters of the measured and simulated j -th layer data can be evaluated by estimating probability distribution using four basic moments: mean, dispersion, skewness, and kurtosis. Using these four moments, the measured histogram and calculated probability density function can be compared to the Gaussian distribution.

Kurtosis allows for estimating the “tails” of the probability density function of the measured dataset. It can be used as a descriptor of the shape of the probability distribution function. A dataset has a distinct peak near the mean when its kurtosis has a high value. The datasets with a flat top near mean kurtosis have a low value. The kurtosis can be defined as the fourth standardized moment and expressed by the following:

$$\beta = \frac{\mu_4}{\sigma^4}, \quad (7)$$

where μ_4 is the fourth moment near the mean, and σ is the standard deviation.

Skewness can be described as a dimensionless parameter estimating the symmetry of the distribution. If the measured dataset distribution function is near ideal symmetry, the skewness value approaches 0. If the measured dataset mean is shifted to the left, this is represented by a negative skewness value, and a shift to the right is represented by a positive skewness value. The skewness can be expressed by the following:

$$\gamma = \frac{\mu_3}{\sigma^3}, \quad (8)$$

where μ_3 is the third moment near the mean, and σ is the standard deviation.

Knowledge about the histogram shape of time error measurements can help to predict time intervals needed for wake-ups of WSN nodes. Packet flight time or time on air (see Figure 4) from point to point can be treated as a constant-known value and can be measured. For the “star” configuration network or sender–receiver network (see Figure 2), the time error impact on the whole network life cycle is not as critical compared to the receiver–receiver (see Figure 1) configuration. If WSN is configured using “star” topology, time error will impact only one wireless node. That is because the “star” network configuration main node or the so-called gateway is responsible for synchronization messages and transfers them directly to wireless nodes using point-to-point (p2p) data exchange principles.

4. Experiments

For evaluation of the synchronization time distributions, the experimental research was performed using the setup (see Figure 6) consisting of two WS nodes, PC, and oscilloscope LeCroy HRO 66Zi. The WS node 1 works as a gateway. It is connected to the host PC via a UART/USB converter for quick setup possibility and state monitoring using a terminal window. WS node 2 works as a wireless node (receiver) and is also connected to the host

PC. Both transceivers have hardware-driven interrupt output pins enabled to form TX Flag and RX Flag signals (see Figure 3).

The availability on the market, presence of the low power mode(s), and end cost were considered as criteria for choosing the transceiver manufacturers and particular devices for the experiment. Three types of transceivers, SX1231 and SX1269 from Semtech Corporation and nRF24L01 from Nordic Semiconductor ASA, were chosen. Modulation types for each transceiver were chosen according to their setup:

- SX1231—OOK (on/off keying), FSK (frequency shift keying) with the Gaussian filter for pulse shaping;
- SX1269—LORA (long-range modulation type with spread spectrum technique), FSK with switchable Gaussian filter;
- nRF24L01—FSK with the Gaussian filter for pulse shaping.

In the experimental setup, as presented in Figure 6, the LeCroy HRO 66Zi oscilloscope was used to acquire time delay measurements between the WS nodes. TX Flag and RX Flag hardware signals were connected to channel 1 and channel 2 of the oscilloscope. The oscilloscope measurement procedure was controlled from a PC using data acquisition software implemented in MATLAB environment via VISA interface.

During the experiment, the transceivers were maintained at constant positions to minimize the time on air variation. The WS node 1 was preprogrammed to send the data packet (fixed payload) with a repetition period of 100 ms. Each time after the data packet is completely sent, the TX Flag is automatically formed by the transceiver hardware. At the receiver side, the hardware-driven RX Flag is configured to change its state (from high to low) when the data packet is received. The received packet state in the transceiver hardware is configured to be set after the preamble and header are found and the CRC of the packet is checked. The time delay measurement using the LeCroy HRO 66Zi oscilloscope between TX Flag and RX Flag was performed on falling edges of the pulse signals generated by hardware interrupts on the transmitter TX Flag and on receiver RX Flag, and the histograms using at least 200,000 measurements were drawn using the MATLAB software. In the following sections, the experimental time delay distributions are presented, and the dependencies on different communication channel setups are analyzed.

4.1. nRF24L01 GFSK

For the first experimental setup, the Nordic semiconductor transceivers nRF24L01 were used. Both transceivers can send data signals from 2400 to 2525 MHz frequency range. Free channels (2402 MHz) for communication at the laboratory were chosen. And for transmission, GFSK modulation was used. Experiments were repeated with three different bitrates: 250 kbps, 1000 kbps, and 2000 kbps. Figure 7 presents the time delay histogram measured between the TX Flag and RX Flag at transceiver pins using different bitrates. As can be seen from the figure, the form of the histograms is similar—two main peaks with varying delays dependent on the packet transfer rate.

For the following experiments, only a bitrate of 2000 kbps was used because, in the authors' opinion, the results using different bitrates would be very similar. Figure 8 presents the simulation results modeled using data received from experimental time delay measurement. The behavior of time delay measured between TX and RX Flag was simulated for receiver–receiver WSN configuration (see Figure 1). Figure 8a represents a histogram modeled using data packet re-transfer through 4 nodes; Figure 8b represents 16 nodes. As can be seen from the presented figure, as the number of nodes increases, the histogram shape becomes similar to a Gaussian distribution.

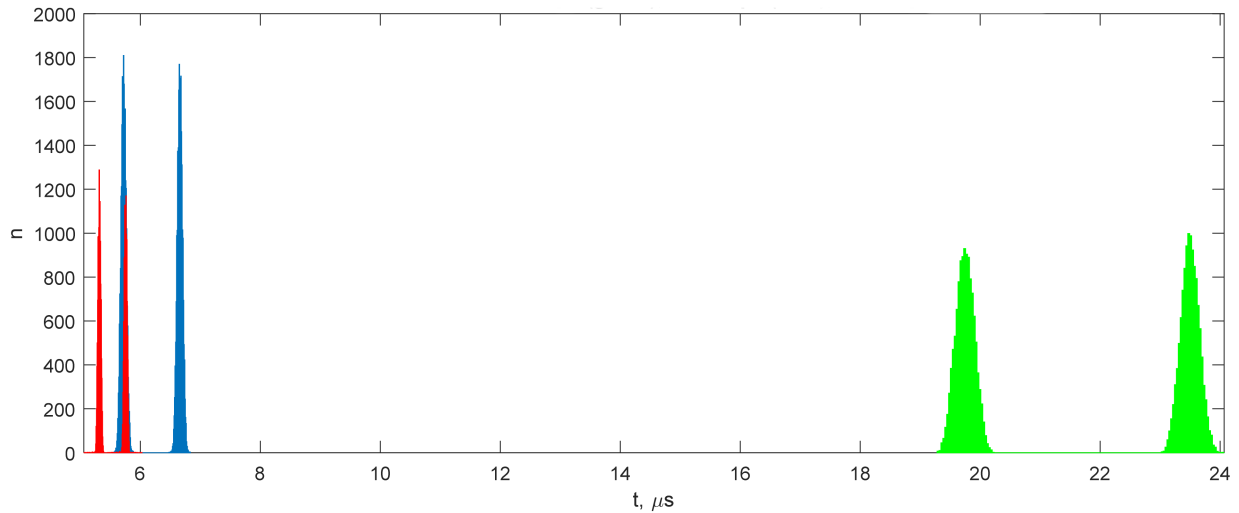


Figure 7. NRF24L01 delay histograms: green—250 kbps; blue—1000 kbps; red—2000 kbps.

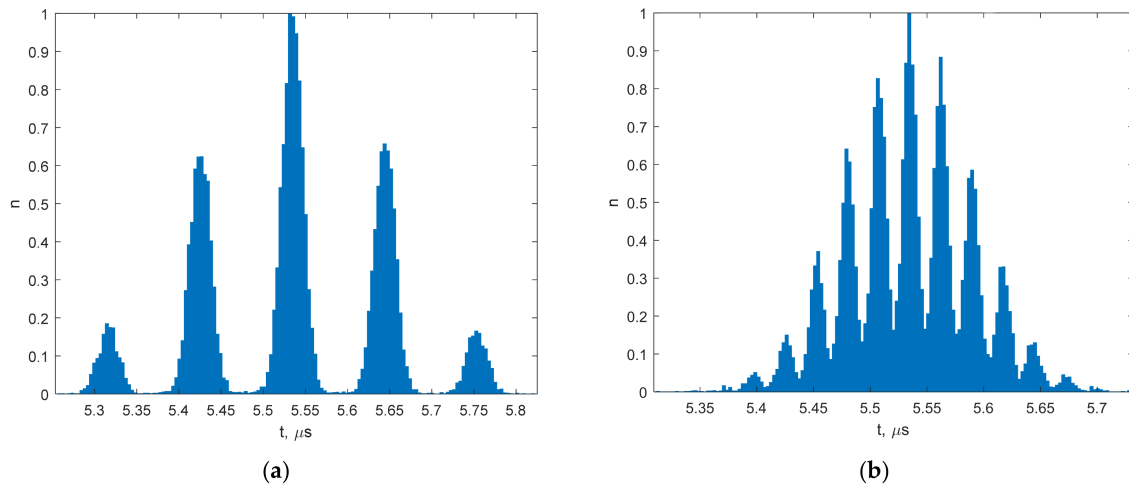


Figure 8. NRF24L01 histogram modeled for data packet re-transfer: (a) through 4 nodes; (b) through 16 nodes.

4.2. SX1276 LORA

For the next experiment, SX1276 transceivers were used. SX1276 IC operates in the ISM band (from 137 to 1020 MHz). The transceiver can send data signals using FSK (various subtypes such as GFSK, MSK, etc.) or long-range spread spectrum modulation LORA. For experiments, an 868 MHz frequency was used. SX1276, when modulating data with LORA, can use different spreading factors (SF6 to SF12). During experiments, some measurement results were analyzed, and it was noticed that time delay does not have a noticeable dependency from using different spreading factors. The results presented as time delay measurement histograms were obtained using the same spreading factor (SF7).

Figure 9 presents experimental measurement results for the WSN configuration presented in Figure 2. It is noticeable that the histogram shape is similar to the uniform distribution. The simulation using experimental measurement data was made for the WSN, which is presented in Figure 1 (receiver–receiver). Modelling two jumps from node to node created a histogram shape similar to a triangle distribution (see Figure 10a), but after the wireless node number was increased to more than 4, the time delay histogram shape changed to Gaussian (see Figure 10b).

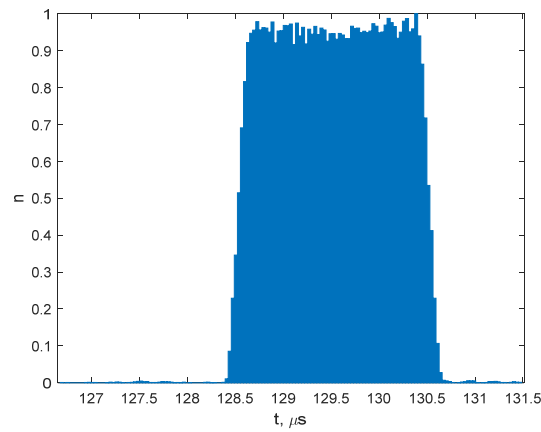


Figure 9. SX1276 LORA histogram measured using point-to-point setup.

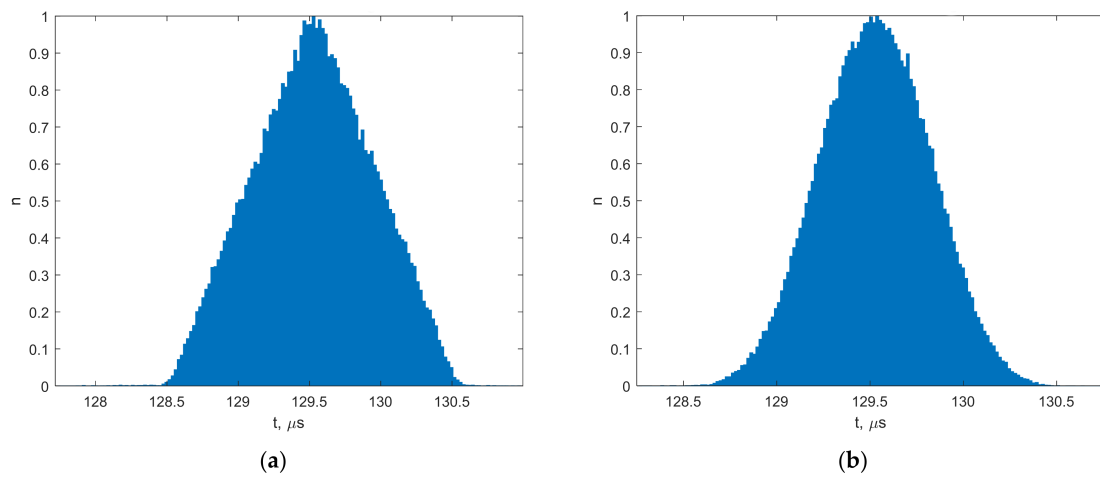


Figure 10. SX1276 LORA histogram modeled for data packet re-transfer: (a) through 2 nodes; (b) through 4 nodes.

4.3. SX1276 FSK

The experiment was repeated using the same chip, SX1276, but with a different modulation type (FSK with a deviation of 25 kHz) for data transmission. Different frequency deviation settings during experiments were tried, but the results showed that the influence of deviation on time delay measurements (between TX and RX flag) was not noticeable. The histogram presented in Figure 11 was created using experimental measurement results.

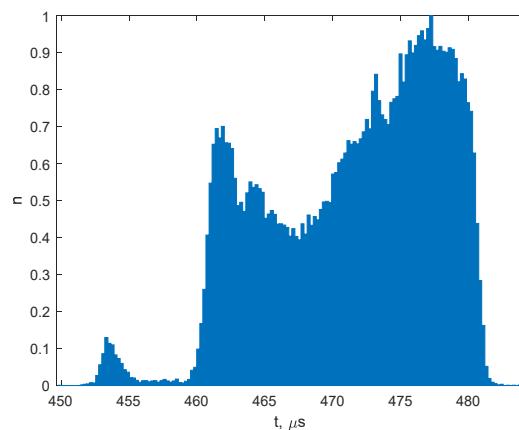


Figure 11. SX1276 FSK histogram measured using point-to-point setup.

Histograms presented in Figure 12 were modeled using jumps through 2 wireless nodes and 4 wireless nodes accordingly. It is noticeable from Figure 12b that with an increased number of jumps from node to node, the histogram shape becomes Gaussian-like.

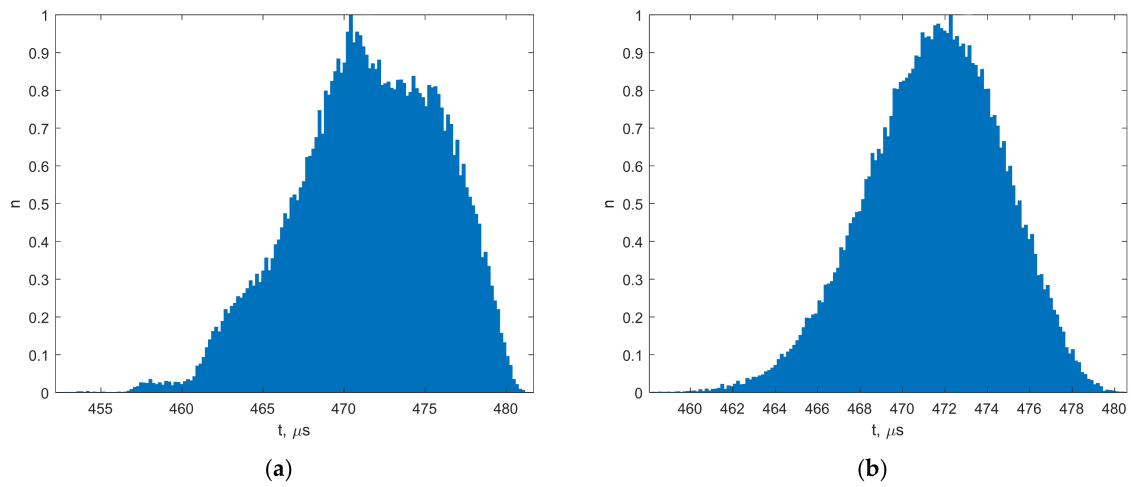


Figure 12. SX1276 FSK histogram modeled for data packet re-transfer: (a) through 2 nodes; (b) through 4 nodes.

4.4. SX1231 OOK

The last experiment was made using an SX1231 pair of transceivers from Semtech Corporation. The receiver can send data using two modulation types: OOK (on-off keying (also called ASK)) and FSK (frequency shift keying). For experiments, OOK modulation with 4800 kHz bitrate was chosen. The histogram created from experimental measurement results is presented in Figure 13.

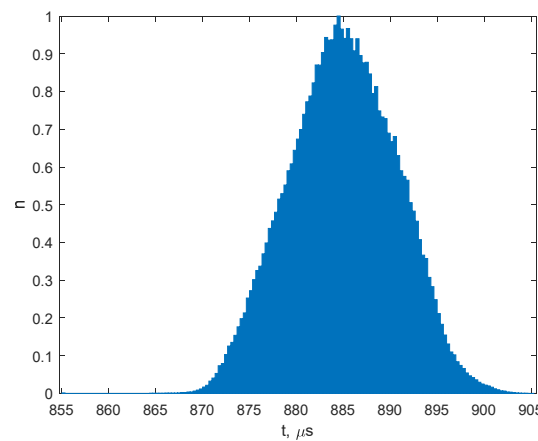


Figure 13. SX1231 OOK histogram measured using point-to-point setup.

Histograms created by simulating data packet transfer through 2 wireless nodes and 4 wireless nodes are presented in Figure 14. It is also noticeable that with an increased number of nodes, histograms resemble a Gaussian-like shape.

Table 1 summarizes measured time delay histograms. The provided data include measured time between two transceivers, TX and RX flags; the travel of the synchronization packet modeled; and the predictable time delay of the WS network estimated. The simulation is performed using Formulas (5) and (6) described in Chapter 3. The dataset size $N = 200,000$ samples for each case. The measured dataset was used for the simulation of the further jumps in the WSN. The jump number given in Table 1 corresponds to the parameter j in Formula (6). The statistical parameters were calculated from the simulated datasets using Formulas (7) and (8).

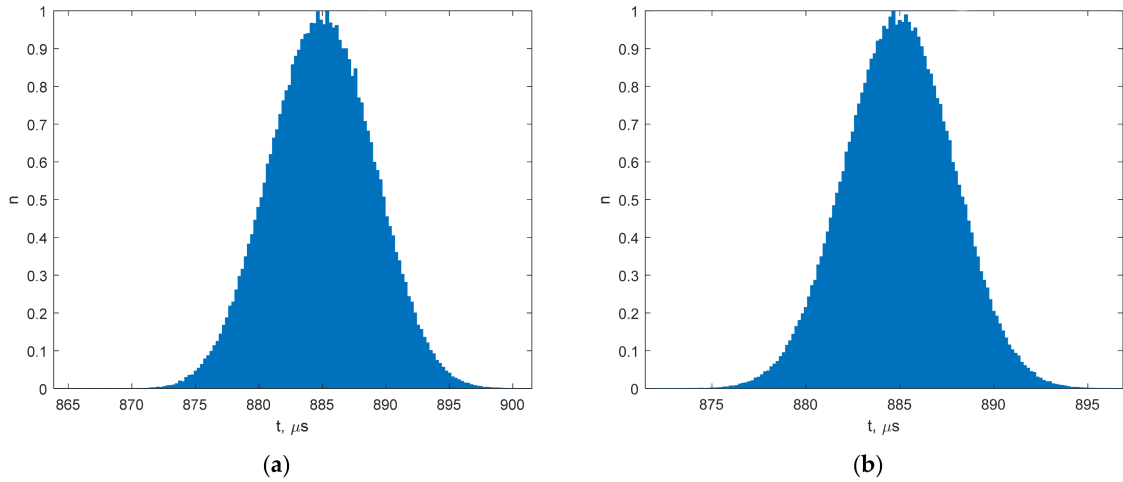


Figure 14. SX1231 OOK histogram modeled for data packet re-transfer: (a) through 2 nodes; (b) through 4 nodes.

Table 1. Summarized data from delay measurements and modeling results.

Transceiver	Modulation	Carrier Freq., MHz	Jump No.	Mean t_{δ_avgj} , μ s	Standard Dev. δ_{TRXj} , μ s	Kurtosis β	Skewness γ
nRF24L01	GFSK	2402	1	5.53	0.22	1.05	0.009
nRF24L01	GFSK	2402	4	5.53	0.11	2.51	−0.010
nRF24L01	GFSK	2402	16	5.53	0.05	2.96	−0.016
SX1276	LORA	868	1	129.53	0.59	1.93	−0.020
SX1276	LORA	868	2	129.53	0.41	2.47	−0.017
SX1276	LORA	868	4	129.53	0.29	2.72	−0.003
SX1276	FSK	868	1	471.48	6.33	2.39	−0.518
SX1276	FSK	868	2	471.50	4.47	2.71	−0.370
SX1276	FSK	868	4	471.47	3.17	2.84	−0.261
SX1231	OOK	868	1	884.96	5.68	2.64	−0.012
SX1231	OOK	868	2	884.96	4.01	2.82	−0.014
SX1231	OOK	868	4	884.96	2.84	2.91	−0.006

After analysis of measured and modeled data, it can be stated that almost all chips using different modulations produce near-symmetrical histograms. Only the SX1276 chip used with FSK modulation created a histogram with the center moved to the right. By means of kurtosis, only the GFSK histogram created using point-to-point measurements stands out. But point-to-point transmission is actually only for star configuration networks. Using mean and dispersion, the wake-up period of wireless sensor nodes can be estimated. It can be considered that after a certain jump number, 1 jump means that the transmitting node sends or resends the synchronization data packet to the receiving node and the t_{δ} measurement histogram becomes Gaussian alike. So, using this assumption, the wake-up time for the sensor network with j layers can be described by the following:

$$t_{wake_upj} = \sum_{k=1}^j \left(t_{\delta_avgj} + k \cdot \delta_{TRXj} - t_{TX_pl} \right), \tag{9}$$

where t_{TX_pl} is TX payload preparation delay, t_{δ_avgj} is the estimated average data packet delay (see Table 1), k is the coverage factor for the j -th WSN layer jitter estimate δ_{TRXj} .

As can be seen from Table 1, different modulation types introduce different delays between the transmitter and receiver. The nRF24L01 chip produces the smallest 5.53 μ s time delay, and SX1231 gives the biggest delay of 884.96 μ s. When comparing different modulations of the same chip, it is noticeable that the SX1276 chip using Lora modulation produces a 129.53 μ s time delay, while using FSK modulation gives about a 3.6 times bigger delay of 471.48 μ s. On the other hand, GFSK (nRF24L01), which is the same FSK as Gaussian prefiltering running at the highest rate, can have a much smaller time delay in

comparison with LORA modulation. Also, with high data rates, the possibility of loose data packets arises. Additionally, difficulties in transferring data using low-power profiles over long distances must be taken into account. All chips, if used for long-range communication, must have a reduced data rate. For example, SX1231 can reach communication distances up to 1000 m using a 600 bps data rate. If the rate is increased to hundreds of kbps, the distance will drop to less than a hundred meters. The only solution for this problem is to increase the TX output power, but the energy consumption would also increase.

During the design stage of low-power WSNs, measured and presented delays must be considered. The operation of low-power networks is mainly based on the idea that the wireless sensor nodes wake up at certain time intervals or on some trigger. This helps to extend the network life cycle working on batteries. If we can reduce waking-up times or extend intervals between wake-ups, we can boost the WSN life cycle.

5. Conclusions

Wireless sensor networks (WSN) are widely used in various areas, including smart water meters, smart electricity metering systems, mine safety systems, etc. However, time synchronization is a major concern when using low-power WSNs for precise measurements.

Various delays can occur when sending a synchronization packet between two nodes in a wireless sensor network (WSN). These delays include the following:

- Send delay: The time it takes for the transmitter node to construct a synchronization message and submit it to the MAC layer;
- Channel access delay: The time it takes for the node to access the channel to transmit the message. This delay is random and depends on the current status of the channel (idle or busy);
- Transmission delay: The time it takes for the message to be transmitted from the transmitter node to the receiver node. This delay depends on the physical layer parameters of the transceiver;
- Propagation delay: The time it takes for the message to travel from the transmitter node's antenna to the receiver node's antenna. This delay is determined by the distance between the two nodes;
- Receive delay: The time it takes for the message to be received and processed by the receiver node. This delay includes the time it takes for the message to be copied from the antenna to the physical layer and the time it takes for the message to be processed by the network stack;
- Processing delay: The time needed to process the received packet.

In the experimental part of this paper, the communication delay measurements and quantitative jitter analysis were performed using different conditions and dependencies from data bitrate and modulation type for different hardware implementations of the WSN. The experimental results showed that different chips and modulation schemes introduce varying delays between transmitter and receiver:

- The nRF24L01 chip with GFSK offers the lowest delay (5.53 μ s), while SX1231 has the highest delay (884.96 μ s);
- Using the same chip, FSK modulation can have a much higher delay compared to the LoRa-SX1276 chip, with FSK experiencing a 3.6 times higher delay (471.48 μ s) than with LoRa (129.53 μ s);

In addition to the type of modulation, data transmission rate and distance must be taken into account. Higher data rates lead to increased packet loss and reduced communication range. For long-range communication, all chips require lower data rates. For example, SX1231 achieves 1000 m at 600 bps but drops below 100 m at hundreds of kbps. Increased TX power can improve range at higher data rates, but this comes at the cost of higher energy consumption.

Selecting the appropriate modulation scheme and optimizing data rates based on the desired range and power consumption are critical for designing efficient low-power WSNs.

This research offered a foundation for optimizing network configuration and parameters to extend the operational life of low-power sensor nodes. However, there are still some existing issues and areas for future research. One of the challenges is the sender-induced delay, which cannot be avoided in sender–receiver synchronization protocols. Future studies could focus on developing protocols or techniques to reduce or eliminate this delay. Another area for future research is the impact of modulation types and data rates on time delay and jitter. The provided study analyzed the differences in time delay induced by different hardware solutions and modulation types, but further investigation can delve deeper into understanding the specific effects of these factors and how they can be mitigated or optimized.

Author Contributions: Conceptualization, D.G. and M.K.; methodology, D.G, M.K. and P.K.; software, G.B. and S.J.; validation, Š.K. and A.M.; formal analysis, A.M. and J.D.; investigation, M.K. and D.G.; writing—original draft preparation, M.K. and P.K.; writing—review and editing, Š.K.; visualization, D.G. and Š.K.; supervision, Š.K. All authors have read and agreed to the published version of the manuscript.

Funding: This research received no external funding.

Data Availability Statement: The data presented in this study are available on request from the corresponding author.

Conflicts of Interest: The authors declare no conflicts of interest.

References

1. Mudumbe, M.J.; Abu-Mahfouz, A.M. Smart water meter system for user-centric consumption measurement. In Proceedings of the 3th International Conference on Industrial Informatics (INDIN), Cambridge, UK, 22–24 July 2015; pp. 993–998.
2. Burunkaya, M.; Pars, T. A smart meter design and implementation using ZigBee based Wireless Sensor Network in Smart Grid. In Proceedings of the 4th International Conference on Electrical and Electronic Engineering (ICEEE), Ankara, Turkey, 8–10 April 2017; pp. 158–162.
3. Xu, H.; Wu, J. Metal mine underground safety monitoring system based on WSN. In Proceedings of the 9th IEEE International Conference on Networking, Sensing and Control, Beijing, China, 11–14 April 2012; pp. 244–249.
4. Knyva, M.; Gailius, D.; Balčiūnas, G.; Pratašius, D.; Kuzas, P.; Kukanauskaitė, A. IoT Sensor Network for Wild-Animal Detection near Roads. *Sensors* **2023**, *23*, 8929. [[CrossRef](#)] [[PubMed](#)]
5. Zhang, K.; Wang, W. The research of environmental monitor system in brewage house of alcohol factory based on WSN. In Proceedings of the 10th World Congress on Intelligent Control and Automation, Beijing, China, 6–8 July 2012; pp. 4401–4404.
6. Kannamma, M.B.; Chanthini, B.; Manivannan, D. Controlling and monitoring process in industrial automation using Zigbee. In Proceedings of the International Conference on Advances in Computing, Communications and Informatics (ICACCI), Mysore, India, 22–25 August 2013; pp. 806–810.
7. Saadaoui, S.; Tabaa, M.; Monteiro, F.; Chehaitly, M.; Dandache, A.; Oukaira, A. IWSN under an industrial wireless channel in the context of Industry 4.0. In Proceedings of the 29th International Conference on Microelectronics (ICM), Beirut, Lebanon, 10–13 December 2017; pp. 1–4.
8. Dandan, P.; Ming, W.; Dongmei, G.; Yaozhang, S. Acoustic emission inspection based on wireless FBG sensing system. In Proceedings of the 10th International Conference on Sensing Technology (ICST), Nanjing, China, 11–13 November 2016; pp. 1–4.
9. Vilhar, A.; Depolli, M. Time synchronization problem in a multiple wireless ECG sensor measurement. In Proceedings of the 14th Annual Conference on Wireless On-Demand Network Systems and Services (WONS), Isola, France, 6–8 February 2018; pp. 83–86.
10. Tashtarian, F.; Montazerolghaem, A.; Abbasi, M. Distributed Lifetime Optimization of Wireless Sensor Networks in Smart Grid. In Proceedings of the IEEE International Conference on Smart Energy Grid Engineering (SEGE), Oshawa, ON, Canada, 12–15 August 2018; pp. 240–243.
11. Klinglmayr, J.; Pichler, M.; Berger, A.; Springer, A.; Potsch, A. Low-Complex Synchronization Algorithms for Embedded Wireless Sensor Networks. *IEEE Trans. Instrum. Meas.* **2014**, *64*, 1032–1042.
12. Baghyalakshmi, D.; Ebenezer, J.; Satyamurty, S.A.V. WSN based temperature monitoring for High Performance Computing cluster. In Proceedings of the 2011 International Conference on Recent Trends in Information Technology (ICRTIT), Chennai, India, 3–5 June 2011; pp. 1105–1110.
13. Li, X.; Chang, C.; Gao, W. Clock synchronization method for star-structure Wireless Sensor Network. In Proceedings of the 2010 International Conference on Computational Aspects of Social Networks, Taiyuan, China, 26–28 September 2010; pp. 603–606.
14. Hwang, S.; Baek, Y. Reliable time synchronization protocol for Wireless Sensor Network. In Proceedings of the 2005 International Conference on Embedded and Ubiquitous Computing EUC'05, Nagasaki, Japan, 6–9 December 2005; pp. 663–672.

15. Maroti, M.; Kusy, B.; Simon, G.; Ledeczi, A. The flooding time synchronization protocol. In Proceedings of the 2nd International Conference on Embedded Networked Sensor Systems (SenSys'04). ACM, Baltimore MD, USA, 3–5 November 2004; pp. 39–49.
16. Elson, J.; Girod, L.; Estrin, D. Fine-grained network time synchronization using reference broadcasts. In Proceedings of the OSDI '02: Proceedings of the 5th Symposium on Operating Systems Design and Implementation, Boston, MA, USA, 9–11 December 2002; pp. 147–163.
17. Kashyap, D.; Jain, T.K. Comparative analysis of time synchronization schemes for Wireless Sensor Networks. In Proceedings of the 2014 International Conference on Signal Propagation and Computer. Technology (ICSPCT 2014), Ajmer, India, 12–13 July 2014; pp. 106–109.
18. Nguyen, V.-H.; Tan, N.D. Voronoi diagrams and tree structures in HRP-EE: Enhancing IoT network lifespan with WSNs. *Ad. Hoc. Netw.* **2024**, *161*, 48185–48196. [[CrossRef](#)]
19. Verma, S.; Kaur, S.; Rawat, D.B.; Xi, C.; Alex, L.T.; Jhanjhi, N.Z. Intelligent Framework Using IoT-Based WSNs for Wildfire Detection. *IEEE Access* **2021**, *9*, 48185–48196. [[CrossRef](#)]
20. Faheem, M.; Kuusniemi, H.; Eltahawy, B.; Bhutta, M.S.; Raza, B. A lightweight smart contracts framework for blockchain-based secure communication in smart grid applications. *IET Gener. Transm. Distrib.* **2024**, *18*, 625–638. [[CrossRef](#)]
21. Nakutis, Ž.; Rinaldi, S.; Kuzas, P.; Lukočius, R. A Method for Noninvasive Remote Monitoring of Energy Meter Error Using Power Consumption Profile. *IEEE Trans. Instrum. Meas.* **2020**, *69*, 6677–6685. [[CrossRef](#)]
22. Kawoosa, A.I.; Prashar, D.; Faheem, M.; Jha, N.; Khan, A.A. Using machine learning ensemble method for detection of energy theft in smart meters. *IET Gener. Transm. Distrib.* **2023**, *17*, 4794–4809. [[CrossRef](#)]
23. Nakutis, Ž.; Daunoras, V.; Rybelis, T.; Kuzas, P.; Jasiūnas, K. Clock Synchronization Accuracy of Power Line Communication Connected Devices: A Case Study. In Proceedings of the 2020 3rd International Colloquium on Intelligent Grid Metrology (SMAGRIMET), Cavtat, Croatia, 20–23 October 2020; pp. 85–90.
24. Kulakli, A.B.; Erciyes, K. Time synchronization algorithms based on Timing-sync Protocol in Wireless Sensor Networks. In Proceedings of the 23rd International Symposium on Computer and Information Sciences, Istanbul, Turkey, 27–29 October 2008; pp. 1–5.
25. Djenouri, D. R⁴ Syn: Relative referenceless receiver/receiver time synchronization in Wireless Sensor Networks. *IEEE Signal Process. Lett.* **2012**, *19*, 19175–19178. [[CrossRef](#)]
26. Liu, C.; Pang, H.; Cao, N. Research on Time Synchronization Technology of Wireless Sensor Network. In Proceedings of the 2017 International Conference on Cyber-Enabled Distributed Computing and Knowledge Discovery (CyberC), Nanjing, China, 12–14 October 2017; pp. 391–394.

Disclaimer/Publisher's Note: The statements, opinions and data contained in all publications are solely those of the individual author(s) and contributor(s) and not of MDPI and/or the editor(s). MDPI and/or the editor(s) disclaim responsibility for any injury to people or property resulting from any ideas, methods, instructions or products referred to in the content.